

Small-scale positioning using digital compasses

Andrei Popleteev
SnT, University of Luxembourg
Luxembourg City, Luxembourg
Email: andrei.popleteev@uni.lu

Hossein Arshad
SnT, University of Luxembourg
Luxembourg City, Luxembourg
Email: hossein.arshad@gmail.com

Vladimir Lutkovski
Belarusian State University
Minsk, Belarus
Email: lutkovski@bsu.by

Abstract—This work-in-progress paper presents a method for precise small-scale localization using the “inverse compass” approach, where stationary magnetometers track the location of a mobile permanent magnet. While current indoor localization systems strive to achieve sub-meter localization performance in rooms and buildings, we highlight the need for a centimeter-level precise localization systems, even with a limited coverage. Experimental evaluation of a prototype system demonstrated 3.4 cm median 3D localization accuracy within the 20x20x10 cm test space.

1. Introduction

The majority of indoor positioning research focuses on providing reliable and accurate localization performance at a scale of a building or an apartment [1]. Typical radio-based systems provide an accuracy of few meters [1], which is sufficient for room-level indoor navigation and general context awareness. However, a number of areas would benefit from more precise localization techniques, even if at smaller scales. Cooking, grooming and gesture-based interactions are some examples of activities which are performed in bounded areas which require precise centimeter-level motion tracking.

Currently these activities can be monitored using video-based approaches [2], [3] which are computationally expensive, sensitive to illumination conditions and may raise privacy concerns [4]. Wearable sensors can provide information about limb motion (acceleration, direction), but not an absolute position in space. Finally, RFID readers can detect presence of RFID tags in their vicinity, but such localization is often too coarse for the mentioned use cases.

This paper explores precise small-scale positioning using magnetic fields. We employed stationary digital magnetometers in order to estimate the location of a permanent magnet, which can be attached to any non-magnetic object (for instance, a magnetic ring on a finger). In this setup, the mobile part does not require batteries, while stationary magnetometer sensors are cheap, power-efficient and fundamentally unable to invade user’s privacy. Experimental evaluation of a simple geometric localization algorithm demonstrated few-centimeters accuracy with minimal computation.

The rest of the paper is organized as follows. The next section provides an overview of related work. Then, we

introduce our approach, present the hardware prototype and results of its experimental evaluation. The paper concludes with a discussion of the advantages and limitations of magnetic tracking, and an outline of the future work.

2. Related Work

Small-scale tracking of motion and human activity have previously been addressed by computer vision, wearable sensors and RFID technology.

Computer vision is widely used for object tracking and recognition of human activity from hand gestures to general daily tasks [5]. Due to the algorithmic complexity of the task, the objects of interest are often tagged with color markers (such as colored glove [6]). The advance of consumer-grade depth-sensing cameras (such as Microsoft Kinect) enriched the researchers with a new dimension for sensing. Such 3D cameras have been successfully applied to hand tracking [7], sign language recognition [6], and tracking of cooking activities [3].

Vision-based methods can achieve sub-millimeter precision of contact-free tracking (for example, Leap Motion controller [2]). However, there are a number of limitations restricting their use in ambient sensing. The cameras need to have a clear view of the tracked area, preferably at a fixed view point with static lighting conditions [5]. Video processing algorithms are resource-intensive and thus are not suitable for battery-powered sensor nodes. Finally, video cameras can be a threat to personal privacy (or at least perceived so), which limits their adoption in smart homes [4].

Alternative approaches to small-scale activity monitoring employ wearable sensors and RFID tracking. Typically, RFID tags are attached to the objects of interest, whereas the user wears a glove [8] or a bracelet [9], [10] with inertial sensors and an RFID reader. Such a setup makes it possible to recognize when the user holds an object, as well as some manipulations performed with the latter. Unfortunately, current wearable devices have rather limited battery life and thus require daily recharging which may not be feasible in assisted daily living scenarios.

Another research direction focuses purely on RFID-based localization [11]. In contrast to the video-based methods, RFID readers do not require line of sight and can identify multiple tags simultaneously. However, since RFID

localization works by detecting the presence of tags within the reader's antenna field, the localization accuracy of such systems is limited by the spatial density of reader antennas which is in turn limited by relatively high costs of the readers.

Magnetic tracking has been introduced as a method for interaction with mobile devices [12], [13]. Recently, magnetic tracking has been proposed as a method for larger-scale indoor activity monitoring with multiple magnetometer sensors [14]. This paper extends [14], moving from coarse-grained detection of magnetic fluctuations around sparsely distributed sensors towards fine-grained magnetic localization using closely collocated magnetometers.

3. Small-scale magnetic positioning

The proposed approach elaborates upon the “inverted compass” concept presented in [14]. The concept enabled coarse-grained localization and activity detection using a wearable permanent magnet and several magnetometer sensors embedded into the environment. When the user passed near one of the sensors, the latter could detect magnetic fluctuations and thus the user's presence. In the present paper, we go further and explore fine-grained localization using actual field strength values reported by collocated magnetometers.

In order to simplify calculations, we made a number of strong assumptions. Firstly, the magnet is considered to be negligibly small in comparison to the compass-to-magnet distances. Secondly, physical dimensions of the compasses are also considered to be negligible and their technical characteristics to be the same. Finally, we kept the the magnet at a distance from the sensors in order to avoid strong saturating fields and possible permanent magnetization of the devices [15, p. 11].

3.1. Physical background

The intensity of a magnetic field H produced by a magnet at a distance d is inversely proportional to d^3 [15, p. 5]:

$$H \sim \frac{M_1}{4\pi\mu_0 d^3} \quad (1)$$

where M_1 is magnetic moment of the magnet and μ_0 is the permeability of vacuum.

Magnetic sensors [16], in turn, measure the magnetic flux density $B = \mu H$, where μ is the magnetic permeability [15, p. 10]. Assuming that the environment, sensors and the magnet do not change, we can combine all the constants into one coefficient β , and express the distance from the readings b_x, b_y, b_z of a three-axis sensor:

$$d = \beta \frac{1}{\sqrt[3]{B}} = \beta \frac{1}{\sqrt[3]{b_x^2 + b_y^2 + b_z^2}} \quad (2)$$

Since all the compasses are assumed to be the same, the value of β depends only on the specific setup and can be

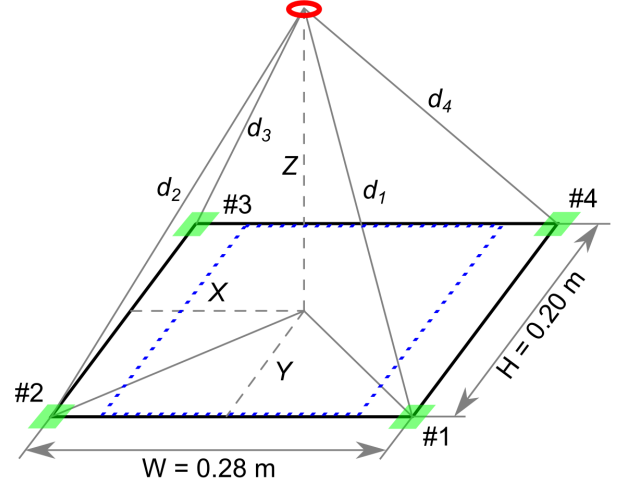


Figure 1. Sensor setup layout. Green squares represent magnetometers, red ring represents the magnet.

calculated using the calibration procedure described below (see Section 3.3).

The sensors are located in the corners of a rectangular area with known dimensions (Figure 1). After trivial geometric transformations, one can express the coordinates of the magnet (x, y, z) using its distance to each compass (d_i).

$$x = \frac{d_1^2 - d_2^2 + W^2}{2W} \quad (3)$$

$$y = \frac{d_2^2 - d_3^2 + H^2}{2H} \quad (4)$$

While these equations include only sensors 1 to 3, similar expressions can be easily derived for any other combination of three sensor. These are omitted here due to space limitations.

In turn, z can be further inferred using 2D coordinates and distance to one of the compasses:

$$z = \sqrt{d_2^2 - x^2 - y^2}, \text{ or} \quad (5)$$

$$z = \sqrt{d_1^2 - (W - x)^2 - y^2}, \text{ or} \quad (6)$$

$$z = \sqrt{d_3^2 - x^2 - (H - y)^2}, \text{ or} \quad (7)$$

$$z = \sqrt{d_4^2 - (W - x)^2 - (H - y)^2} \quad (8)$$

3.2. Ambiguity resolution

Despite the initial assumptions, in real world magnetometer measurements are subject to noise and have limited resolution. This leads to discrepancies in measured d_i distances, so that different combinations of compasses result in different calculated position. Due to the inverse cubic relationship presented in Equation 2, distance estimates are more reliable in proximity to the sensor.

Considering the above, conflicting coordinate estimates from Equations 3 and 5 are combined using weighted average of the candidate values, with weights defined as $1/d_i$, so that more reliable readings are given more weight.

3.3. Calibration

The calibration is performed in two steps. First of all, we take into account background magnetic fields, such as the planet’s own field and local magnetic anomalies. In this phase, the magnet is taken away and all sensor readings are recorded as the initial bias value. This value will then be removed from all future raw readings.

Then, the system evaluates the value of β for the given setup. The magnet is placed in the center of the monitored area, in-plane with the sensors. Since both ground-truth location of the magnet and sensor readings are known, the calibration constant β can be easily inferred from the Equation 2. In contrast to our initial assumption, these values slightly differ between sensors, so the common constant is calculated as the average of the candidate values.

4. Experimental evaluation

This section presents the prototype system, experimental setup and performance evaluation results.

4.1. Prototype

The proposed approach has been evaluated with a custom-built hardware prototype made from off-the-shelf electronic components. Initially we used three digital magnetometers HMC5883L [16], since theoretically three sensors are sufficient for 3D localization (see Equations 3 and 5). However, early experiments demonstrated accuracy degradation in the area without a sensor, so we added the fourth magnetometer. Due to logistic reasons, it was an LSM303DLHC [17] which has the same technical characteristics as the HMC5883L, but features an additional integrated accelerometer (which was not used in our experiments). As the sensors are controlled via the I^2C bus and have the same address, they were connected to an I^2C multiplexer TCA9548A [18], which was queried by a Raspberry Pi [19] board running a data collection script written in Python.

Sensor breakout boards were pinned into a sheet of foamy plastic and encased into a 1-mm thick cardboard box (see Figure 2). The layout and dimensions of the prototype correspond to those shown in Figure 1. The foam ensured that the sensors are as close to the surface of the box as possible. The 12-bit analog-to-digital converters of HMC5883L and LSM303DLHC were configured for 4.0 Ga range with sensitivity of 440 least-significant-bits (LSb) per Gauss.

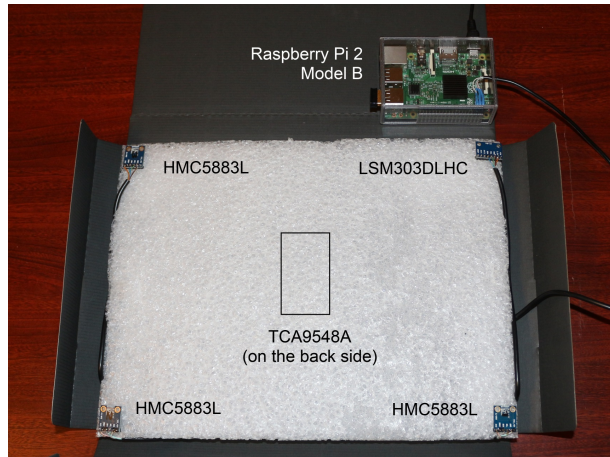


Figure 2. Hardware prototype (opened).

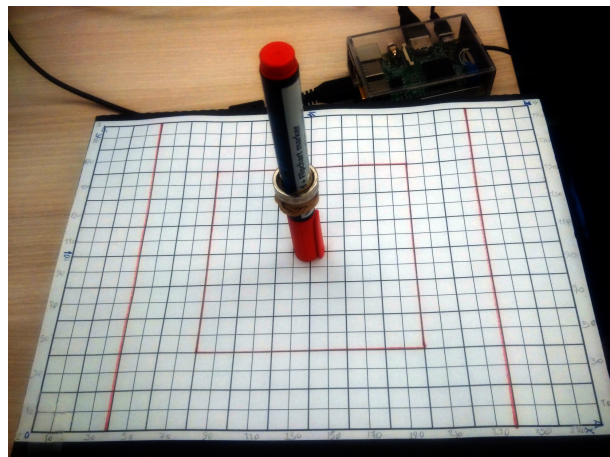


Figure 3. Experimental setup. Magnetic ring is fixed at the required height using a plastic whiteboard marker.

4.2. Experimental setup

The measurements were performed with a 22-mm magnetic ring; due to the generic origins of the sample, its other technical characteristics were not available. The ring was fixed on a plastic whiteboard marker, which enabled us to specify ground-truth 3D location of the magnet with approximately 5 mm precision.

Before data acquisition, the sensors were calibrated to remove the influence of background magnetic fields (see Section 3.3). To avoid sensor saturation, measurements were confined to the central 200×200 mm square of the prototype (blue dotted area in Figure 1). Vertical coordinates ranged from 0 to 100 mm. All measurements were performed along a 20-mm grid for each coordinate, resulting in $10 \times 10 \times 6 = 600$ locations. For each location we recorded raw readings of all the sensors. Calibration data for the β coefficient (see Section 3.3) was recorded separately in the beginning of the session and processed offline during the data analysis.

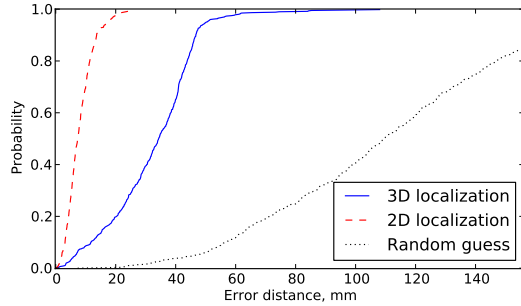


Figure 4. Localization performance of the system.

4.3. Results

Figure 4 demonstrates the localization performance of the 4-sensor setup. Black dotted line is a baseline reference, representing an algorithm returning random coordinates uniformly distributed within the measurements area. Median error distance in 3D space was 34 mm (50 mm at 95% level).

Interestingly, the main source of localization error is the z coordinate (Figure 5). If the z component is excluded from the error distance calculation, the median error of the resulting 2D localization system improves from 34 mm to only 7 mm (17 mm at 95% level), as can be seen in Figure 4. One might assume that the error increases at higher z levels, as the magnet moves further from all sensors. However, Figure 6 demonstrates this is not the case and the localization error does not have a clear dependency on the z level. The plot also suggests that the increased 3D localization error could be attributed to the relatively small errors in 2D position estimate, which are further “amplified” by squaring in Equation 5. According to the same equation, another source of the z error can be imprecise calibration which results in inaccurate estimation of the distances.

One of the possible ways to reduce the localization error, especially along the z axis, is to add an off-plane sensor. While this might not be feasible in some scenarios (for instance, cooking with sensors beneath the table surface), the increased accuracy could be beneficial for interaction and gesture recognition in controlled environments. Performance evaluation of such a setup is beyond the scope of the present proof-of-the-concept paper and remains open for future work.

5. Discussion and Future Work

As any other approach, small-scale magnetic positioning has its strengths and weaknesses.

On one hand, the limited resolution of the sensors restricts the maximum operating range of the system to about 1 m when used with a strong rare-earth magnet [14]. In addition, the magnetometers must be stationary and are nevertheless susceptible to fluctuations of the background magnetic fields and high-power electric appliances operating

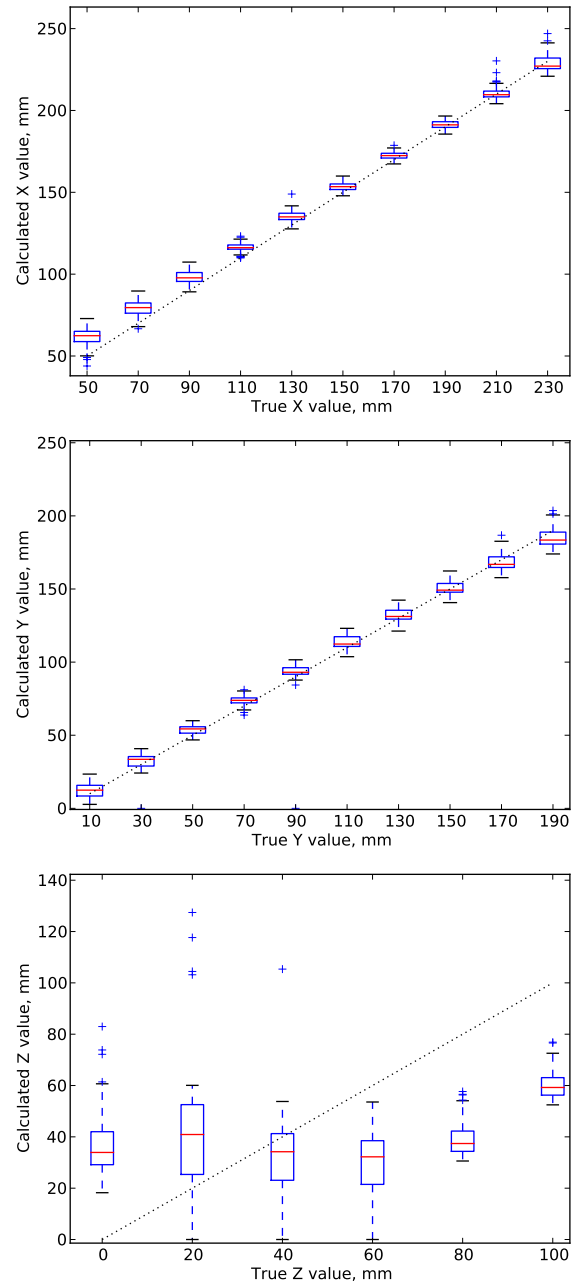


Figure 5. Estimated coordinates compared to ground truth values. Dotted black lines represent ground truth reference.

nearby. Also, in the current implementation, the system can track only one magnet/object and is fundamentally unable to recognize its identity.

On the other hand, permanent magnets do not require batteries and can be integrated into the objects of interest or safely [20] worn as a ring or a bracelet. Stationary magnetometers are small, do not require line of sight and can be easily hidden within the environment. The amount

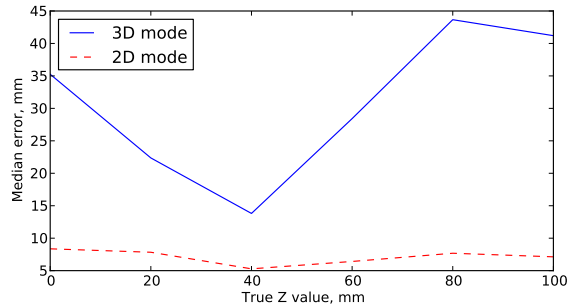


Figure 6. Median error for locations at a given Z level.

of data and the processing algorithm are lightweight and can easily be implemented on an embedded platform. In contrast to video-based methods, magnetic localization is fundamentally unable to capture images and thus intrude user's privacy. Finally, our method could provide a quick and simple solution for non-standard scenarios, such as animal behavior tracking.

While the coverage area of the presented system is rather limited, it can be increased by installation of additional sensors. The system naturally integrates with the larger-scale magnetic localization system presented in [14]. We are currently evaluating the scalability and performance limits of the system and exploring possible applications in ambient interaction and augmented reality.

References

- [1] H. Liu, H. Darabi, P. Banerjee, and J. Liu, "Survey of wireless indoor positioning techniques and systems," *IEEE Transactions on Systems, Man, and Cybernetics, Part C: Applications and Reviews*, vol. 37, no. 6, pp. 1067–1080, 2007.
- [2] F. Weichert, D. Bachmann, B. Rudak, and D. Fisseler, "Analysis of the accuracy and robustness of the Leap Motion controller," *Sensors*, vol. 13, no. 5, pp. 6380–6393, 2013.
- [3] J. Lei, X. Ren, and D. Fox, "Fine-grained kitchen activity recognition using RGB-D," in *Proceedings of the 2012 ACM Conference on Ubiquitous Computing (UbiComp 2012)*. ACM, 2012, pp. 208–211.
- [4] D. J. Cook and N. Krishnan, "Mining the home environment," *Journal of intelligent information systems*, vol. 43, no. 3, pp. 503–519, 2014.
- [5] R. Poppe, "A survey on vision-based human action recognition," *Image and vision computing*, vol. 28, no. 6, pp. 976–990, 2010.
- [6] Z. Zafrulla, H. Brashear, T. Starner, H. Hamilton, and P. Presti, "American sign language recognition with the Kinect," in *Proceedings of the 13th international conference on multimodal interfaces*. ACM, 2011, pp. 279–286.
- [7] M. Van den Bergh and L. Van Gool, "Combining RGB and ToF cameras for real-time 3D hand gesture interaction," in *IEEE Workshop on Applications of Computer Vision (WACV)*. IEEE, 2011, pp. 66–72.
- [8] Z. Ju and H. Liu, "Human hand motion analysis with multisensory information," *IEEE/ASME Transactions on Mechatronics*, vol. 19, no. 2, pp. 456–466, 2014.
- [9] M. Buettner, R. Prasad, M. Philipose, and D. Wetherall, "Recognizing daily activities with RFID-based sensors," in *Proceedings of the 2009 International Conference on Ubiquitous Computing (UbiComp 2009)*. ACM, 2009, pp. 51–60.
- [10] T. Stiefmeier, D. Roggen, G. Ogris, P. Lukowicz, and G. Tröster, "Wearable activity tracking in car manufacturing," *IEEE Pervasive Computing*, no. 2, pp. 42–50, 2008.
- [11] L. M. Ni, D. Zhang, and M. R. Souryal, "RFID-based localization and tracking technologies," *Wireless Communications, IEEE*, vol. 18, no. 2, pp. 45–51, 2011.
- [12] S. Afshari, A. Popteev, R. McCall, and T. Engel, "Magnetic interaction with devices: A pilot study on mobile gaming," in *Proceedings of the 8th Nordic Conference on Human-Computer Interaction (NordCHI 2014)*. ACM, 2014, pp. 891–894.
- [13] H. Ketabdari, K. A. Yüksel, and M. Roshandel, "MagiTact: Interaction with mobile devices based on compass (magnetic) sensor," in *Proceedings of the 15th International conference on Intelligent User Interfaces (IUI 2010)*. ACM, 2010, pp. 413–414.
- [14] A. Popteev, "Activity tracking and indoor positioning with a wearable magnet," in *UbiComp/ISWC 2015 Adjunct proceedings*, Osaka, Japan, Sep. 7–11 2015, pp. 253–256. [Online]. Available: <http://doi.acm.org/10.1145/2800835.2800938>
- [15] S. Chikazumi, *Physics of Ferromagnetism*, 2nd ed., C. D. Graham, Ed. Oxford University Press, 2009, no. 94.
- [16] *Datasheet: Three-axis digital compass IC HMC5883L*, Honeywell International Inc., 2010.
- [17] *Datasheet: Ultra-compact high-performance eCompass module: 3D accelerometer and 3D magnetometer LSM303DLHC*, STMicroelectronics, 2013.
- [18] *Datasheet: TCA9548A Low-voltage 8-channel I²C switch with reset*, Texas Instruments, 2015.
- [19] Raspberry Pi Foundation, "Raspberry Pi 2 model B," Online: <https://www.raspberrypi.org/products/raspberry-pi-2-model-b/>, 2015.
- [20] J. F. Schenck, "Safety of strong, static magnetic fields," *Journal of magnetic resonance imaging*, vol. 12, no. 1, pp. 2–19, 2000.